

Electronic contribution to the enhancement of the ferromagnetic ordering temperature by Si substitution in $\text{Gd}_5(\text{Si}_x\text{Ge}_{1-x})_4$

Y. C. Tseng,^{1,2,*} D. Paudyal,³ Ya. Mudryk,³ V. K. Pecharsky,^{3,4} K. A. Gschneidner, Jr.,^{3,4} and D. Haskel²

¹*Department of Materials Science and Engineering, National Chiao Tung University, Hsin-Chu City, Taiwan*

²*Advanced Photon Source, Argonne National Laboratory, Argonne, Illinois 60439, USA*

³*Ames Laboratory, U.S. Department of Energy, Iowa State University, Ames, Iowa 50011-3020, USA*

⁴*Department of Materials Science and Engineering, Iowa State University, Ames, Iowa 50011-2300, USA*

(Received 4 July 2013; published 29 August 2013)

By using a combination of x-ray spectroscopic and diffraction measurements at high pressures together with density functional theory (DFT) calculations, we show that the increase in Curie temperature T_C , induced by Si substitutions in $\text{Gd}_5(\text{Si}_x\text{Ge}_{1-x})_4$ giant magnetocaloric materials is predominately electronically driven as opposed to lattice driven. Whereas, a lattice contraction with applied pressure increases the strength of exchange (magnetic) interactions between Gd spins, leading to a modest increase in T_C at a rate of $1.2 \text{ K}/\text{\AA}^3$, much larger enhancements in T_C are obtained with Si doping for the same volume reduction ($13.5 \text{ K}/\text{\AA}^3$), indicating that volume (lattice) effects are secondary. Similarly, an orthorhombic [*O*(II)] to monoclinic (*M*) structural phase transition is observed to take place with applied pressure in the paramagnetic state of a $\text{Gd}_5(\text{Si}_{0.125}\text{Ge}_{0.875})_4$ sample at room temperature at a much smaller volume than needed to drive the same structural transition with Si doping, indicating that, even in the absence of magnetic order, electronic effects with Si doping dominate the energetics of structural transformations over lattice (volume) effects. DFT calculations show that the electronic mechanism behind this effect is a stronger Si 3*p*-Gd 5*d* than Ge 4*p*-Gd 5*d* hybridization, a critical ingredient in mediating indirect exchange interactions between localized Gd 4*f* spins. The results highlight the strong sensitivity of the magnetic ordering temperature to the nature of *p-d* hybridization, opening opportunities for tailoring the magnetocaloric properties of these compounds by substituting other *p* and rare-earth elements at the Si/Ge and Gd sites, respectively.

DOI: [10.1103/PhysRevB.88.054428](https://doi.org/10.1103/PhysRevB.88.054428)

PACS number(s): 75.30.Sg

I. INTRODUCTION

Magnetic refrigeration is an attractive energy conversion technology that enables cooling by exposing magnetic materials at temperatures close to their magnetic ordering temperature to a change in the external magnetic field. This technology is more efficient than the conventional vapor-pressure cycle, and no greenhouse gases are needed in the process.¹⁻³ $\text{Gd}_5(\text{Si}_x\text{Ge}_{1-x})_4$ is the most studied pseudobinary system among the $R_5(T)_4$ family of intermetallic compounds (*R* is a rare-earth, and *T* is a group of 13–15 elements)³⁻⁵ due to its giant magnetocaloric effect (GMCE) that is observed near T_C and is tunable by *x*(Si) from nearly absolute zero to near room temperature. Understanding the mechanism behind the increase in the T_C of $\text{Gd}_5(\text{Si}_x\text{Ge}_{1-x})_4$ with Si doping is essential for improving the magnetocaloric properties of these and related materials. The precise mechanism behind this increase remains unclear. It is generally believed that the nearly linear increase in T_C originates from the lattice contraction induced by substituting smaller Si atoms for Ge atoms, which enhances the strength of (indirect) exchange interactions within and between the Gd-containing slabs, therefore, leading to higher ordering temperatures. Although previous papers have demonstrated⁶⁻⁹ that both applied pressure and Si doping result in enhancements of the ferromagnetic (FM) ordering temperature, it was also noted that Si substitution for Ge is a more effective driver of the T_C increase compared to the isotropic mechanical contraction by applied hydrostatic pressure. The addition of Si can result in: (i) nonrandom atomic substitution among the three inequivalent Si/Ge sites,¹⁰ leading to a different lattice response than with applied pressure,

(ii) volume-independent electronic modification, arising from the nature of Si 3*p* compared to Ge 4*p* wave functions resulting in modified magnetic interactions via 3*p*/4*p*–5*d* orbital hybridization, and (iii) local lattice contraction around Si atoms being larger than the macroscopic lattice contraction. These factors could influence the magnetic interactions in a rather complex way, both within and between, the Gd-containing slabs, resulting in different rates of enhancement of FM order with Si substitution and applied pressure. Thus, it is plausible to suggest that the enhancement of T_C with Si doping in $\text{Gd}_5(\text{Si}_x\text{Ge}_{1-x})_4$ is not solely a volume-dependent phenomenon, with the extent of an electronic contribution to such enhancement remaining an important question that needs to be rigorously addressed.

The valence electronic concentration (VEC) theory has been instrumental in explaining how the nominal valence of elements substituting either Ge or R in R_5T_4 compounds is affecting their crystal structure.¹¹⁻¹³ It was shown that, indeed, the change in valence electron count may result in a structural transformation even when the unit-cell volume change is negligible. However, the VEC theory employs an overly simplistic Zintl-Klemm formalism and is not suited to analyze electronic effects that take place when Ge is substituted by isoelectronic Si. Moreover, it is important to consider not only what element is used for the substitution, but also in which atomic position it is located.¹⁴ At the same time, density functional theory (DFT) complemented by thorough experimental examination seems to be well positioned to analyze the site-sensitive electronic effects of isoelectronic substitution.

The questions posed above have implications for the development of magnetic cooling based on these and related

alloys since the highest T_C achieved in these compounds with Si doping in the presence of a GMCE is ~ 280 K (at $x = 0.5$), i.e., remains slightly below room temperature. As a result of decoupling of magnetic and structural transitions above $x = 0.5$, the magnetocaloric effect becomes conventional and, therefore, is significantly reduced.^{2,5} A pathway for more efficient T_C enhancement through chemical substitution is unclear due to incomplete understanding of doping effects other than the volume contraction. In this paper, we present a comparative study of the increase in T_C with Si doping and applied pressure for a given volume change allowing separation of lattice and electronic effects upon exchange interactions.

II. EXPERIMENTAL DETAILS AND METHODS

Polycrystalline samples of $\text{Gd}_5(\text{Si}_x\text{Ge}_{1-x})_4$ with $x = 0.125$ and $x = 0.5$ were prepared at Ames Laboratory as described in Ref. 15. The experimental data were collected at the Advanced Photon Source, Argonne National Laboratory. Ambient-pressure x-ray absorption near-edge structure (XANES) and x-ray magnetic circular dichroism (XMCD) measurements at Si and Ge K edges ($1s \rightarrow 3p/4p$ electric dipole transition) were carried out at beamlines 4-ID-C and 4-ID-D, respectively, with a 4-T magnetic field (H) applied along the x-ray photon wave vector. These XMCD measurements probe magnetic polarization in Si $3p$ (Ge $4p$) states induced by hybridization with polarized Gd $5d$ states. The XANES and XMCD spectra for the $x = 0.5$ sample at ambient pressure were simulated using the FDMNES code within the muffin-tin approximation^{16,17} in order to understand the effect of a local lattice contraction upon the electronic structure. In the simulations, crystallographic information for the $x = 0.5$ sample, determined from x-ray diffraction at ambient conditions, was employed,¹⁰ and initial electronic configurations of $[\text{Xe}]4f^75d^16s^2$, $[\text{Ar}]3d^{10}4s^24p^2$, and $[\text{Ne}]3s^23p^2$ were first assigned to Gd, Ge, and Si, respectively. Slight modifications to these configurations were also tested against the experimental XANES/XMCD data.

High-pressure Gd L_3 edge XMCD measurements ($2p_{3/2} \rightarrow 5d$ transition) were carried out as a function of temperature at beamline 4-ID-D. A diamond-anvil cell (DAC) with perforated diamond anvils was used for these measurements, which allows reducing the attenuation of the x-ray beam intensity in the diamond anvils at the relatively low x-ray energy of the Gd L_3 absorption edge (7.243 keV). An applied magnetic field of $\mu_0 H = 0.7$ T was used for these measurements, which yielded pressure-induced changes in T_C (Refs. 6,7, 18, and 19). Si and Ge K -edge x-ray absorption fine-structure (XAFS) spectra were collected at ambient pressure at beamlines 4-ID-C and 4-ID-D, respectively. These measurements were carried out on a sample with $x = 0.5$ and yielded local structure information for Si and Ge sites. FEFF6.0 theoretical standards²⁰ and the IFEFFIT package²¹ were used to fit the XAFS data. The model includes contributions from the first two atomic shells and distinguishes between correlations involving Si atoms alone (Si-Si and Si-Gd distances) and those involving Ge atoms alone (Ge-Ge and Ge-Gd distances). Although the Si/Ge site occupancies determined from single-crystal diffraction¹⁰ show a small preference for Si atoms to occupy intraslab sites, the XAFS model assumed a random distribution of Si/Ge atoms

among the three inequivalent crystal sites. This is required to limit the number of fitted structural parameters below the number of independent points in the XAFS data. Fits were carried out simultaneously for both edges with Si-Ge bond parameters constrained to be the same for Ge and Si XAFS data. XAFS data in the $(2-10) \text{ \AA}^{-1}$ k range (k is photoelectron wave number) were Fourier transformed, and fits were carried out in real space within the $(2-4.2) \text{ \AA}$ range.

High-pressure angle-dispersive x-ray powder diffraction (XRD) measurements using a Mao-type symmetric DAC²² were carried out at beamline 16-ID-B at room temperature to probe for pressure-induced structural changes, including changes in lattice constants. The collected two-dimensional diffraction rings were integrated with the FIT2D program²³ into diffraction patterns of intensity versus 2θ . Rietveld refinements²⁴ were used to determine crystallographic structures and lattice constants. Local spin-density approximation calculations including on-site Coulomb repulsion parameter U (LSDA + U) (Refs. 25 and 26) within tight-binding linear muffin-tin orbital and full potential linearized augmented plane waves were employed to understand the effect of Si substitution upon p - d hybridization and the effect of local lattice relaxation around Si atoms.

III. RESULTS AND DISCUSSION

Figure 1(a) shows room-temperature XRD patterns for the $x = 0.125$ sample at selected pressures. The $x = 0.125$ sample displays an orthorhombic $O(\text{II})$ phase at ambient pressure where all Gd-containing slabs are disconnected (Si/Ge-Si/Ge interslab bonding broken). Pressures to about 5 gigapascal (GPa) preserve the $O(\text{II})$ structure, albeit with uniformly reduced lattice parameters. Coexistence of $O(\text{II})$ and monoclinic (M) phases is observed in the 5–8 GPa pressure range, and the transition to a single phase M phase is completed above this range (in the M phase, half the Gd-containing slabs are connected). The results of Rietveld refinements to the mixed-phase data at a pressure of 7 GPa are highlighted in Fig. 1(b) where a 75% M -25% $O(\text{II})$ mixture is found. A similar quality of fit is obtained at other pressures. The results show that, at room temperature, the applied pressure yields an $O(\text{II}) \rightarrow M$ structural phase transition, much like Si doping does.^{3,15} This significant result [up to now only $O(\text{II})$ - $O(\text{I})$ and M - $O(\text{I})$ structural phase transitions have been reported to occur with temperature, pressure, or magnetic field in the $\text{Gd}_5(\text{Si}_x\text{Ge}_{1-x})_4$ system] shows that the crystal structure of the $x = 0.125$ sample responds to applied pressure differently at temperatures far above $T_C = 77$ K, compared to below this temperature where pressure further stabilizes the $O(\text{I})$ -FM phase. Clearly, in the presence of magnetic interactions, the end result of any magnetostructural transformation in the $\text{Gd}_5(\text{Si}_x\text{Ge}_{1-x})_4$ system is the $O(\text{I})$ phase as the stable ground-state (low-temperature) structure. However, when magnetism is not playing a role, a more gradual structural evolution from the large volume $O(\text{II})$ structure to the low volume $O(\text{I})$ structure takes place via the formation of the intermediate monoclinic phase as a function of both Si substitution and application of hydrostatic pressure.

Figure 2 describes the details of pressure-induced changes in lattice constants below and above the phase transition with

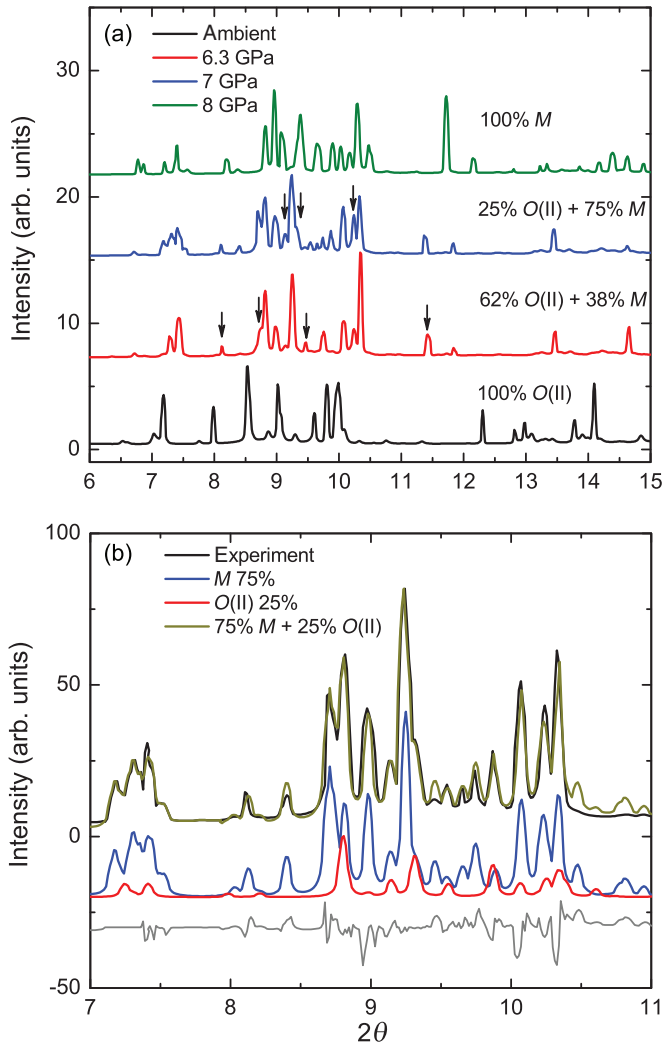


FIG. 1. (Color online) (a) Comparison of XRD patterns at selected pressure points for the $x = 0.125$ sample. The fitted fractional volumes in the mixed-phase region are indicated. The arrows indicate the minority M phase at $P = 6.3$ GPa and the $O(II)$ phase at $P = 7$ GPa. (b) XRD pattern of the $x = 0.125$ sample at $P = 7$ GPa together with results of the Rietveld refinement using a mixture of $O(II)$ and M phases. The gray line at the bottom of the plot represents the difference between the experimental and the theoretical (sum) intensities. The fitted monoclinic angle (γ) of the M phase is 93.05 (2°).

the inset showing the volume fraction of the M phase as a function of applied pressure. In order to compare the effects of applied pressure and Si doping upon the lattice structure, we plot the change in lattice constant versus unit-cell volume in Fig. 3 (the Si-concentration-dependent lattice parameters and unit-cell volumes are taken from Ref. 15). The main panel (a) shows data up to 5 GPa (equal to a unit-cell volume of 837 \AA^3), i.e., before the occurrence of the $O(II) \rightarrow M$ transition, for the purpose of having a clear comparison with Si-doping effects within the $O(II)$ phase. The inset in panel (a) of Fig. 3 shows changes in lattice constants within the M phase for volume contraction down to 790.9 \AA^3 (8 GPa). Panel (b) in Fig. 3 shows Si-doping data up to $x = 1.0$ ($V = 854 \text{ \AA}^3$), displaying $O(II)$ ($0 \leq x \leq 0.3$), $O(II) + M$ ($0.3 < x < 0.43$), M ($0.43 \leq x \leq 0.5$), and finally, the $O(I)$ phase ($0.5 < x \leq 1.0$) as

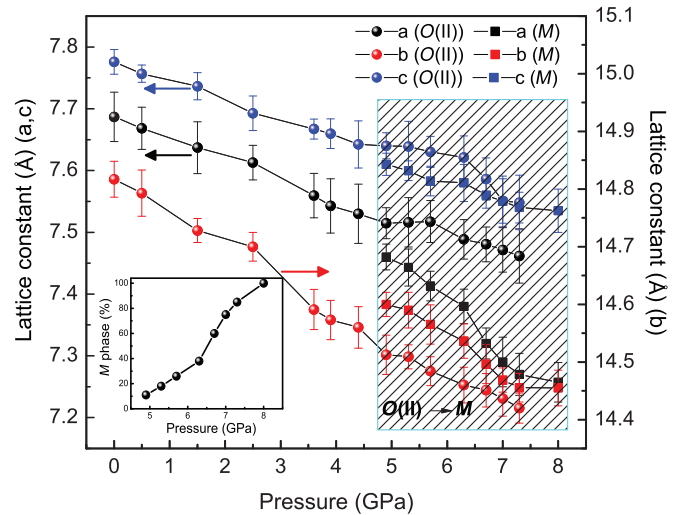


FIG. 2. (Color online) Pressure dependence of three lattice constants from ambient to 8 GPa for the $x = 0.125$ sample. Scalings of the a and c axes are shown on the left-vertical axis, and scaling of the b is shown on the right-vertical axis. The shadowed area highlights the $O(II)$ (circle) \rightarrow M (square) phase transition range where both $O(II)$ and M phases coexist. The inset displays the pressure-dependent volume fraction (in. %) of the M phase from 5 to 8 GPa.

reported in Ref. 15. The volume-dependent magnetic ordering temperatures T_C obtained with applied pressure [panel (c)] or Si substitution [panel (d)] as independently determined by XMCD (pressure)⁶ and superconducting quantum interference device (Si-doping)¹⁵ data are also plotted in Fig. 3. Note that the structural parameters shown in Fig. 3 are room-temperature values obtained from both pressure- and Si-doping experiments.

As seen in Fig. 2, the pressure-induced phase transition is found to take place at ~ 5 GPa in excellent agreement with Ref. 6. The $O(II)$ phase displays isotropic compression with pressure with the three lattice constants exhibiting a similar contraction as seen in panel (a) of Fig. 3. This is not the case in the M phase where pressure induces anisotropic lattice contraction with a larger compressibility along the a axis. Similar behavior is observed with Si doping as shown in panel (b) of Fig. 3. This suggests that, macroscopically, pressure and Si doping contract the lattice in a similar way and implies that deviations in Si/Ge site occupancies from a random distribution are not large in agreement with diffraction results.¹⁰ The results also support the picture of a martensiticlike $O(II) \rightarrow M$ transition requiring a significant shear displacement along the a axis.^{2,3,26} Nevertheless, a much smaller volume contraction is needed with Si doping (relative to pressure) to trigger and to complete the $O(II) \rightarrow M$ phase transition. Volume changes of $\Delta V \sim -6$ and $\sim -50 \text{ \AA}^3$ are needed to drive the $O(II)$ phase into a mixed $O(II) + M$ phase with Si doping and pressure, respectively, whereas, volume changes of $\Delta V \sim -11 \text{ \AA}^3$ and more than -100 \AA^3 (limited by the highest pressure measured) are needed to obtain a single M phase with Si doping and pressure, respectively. Besides, for a given volume change, Si doping yields a dT_C/dV of 13.55 K/\AA^{-3} across $O(II)$, $O(II) + M$, and M phases, which is much larger than 1.2 K/\AA^{-3} yielded by pressure as shown by

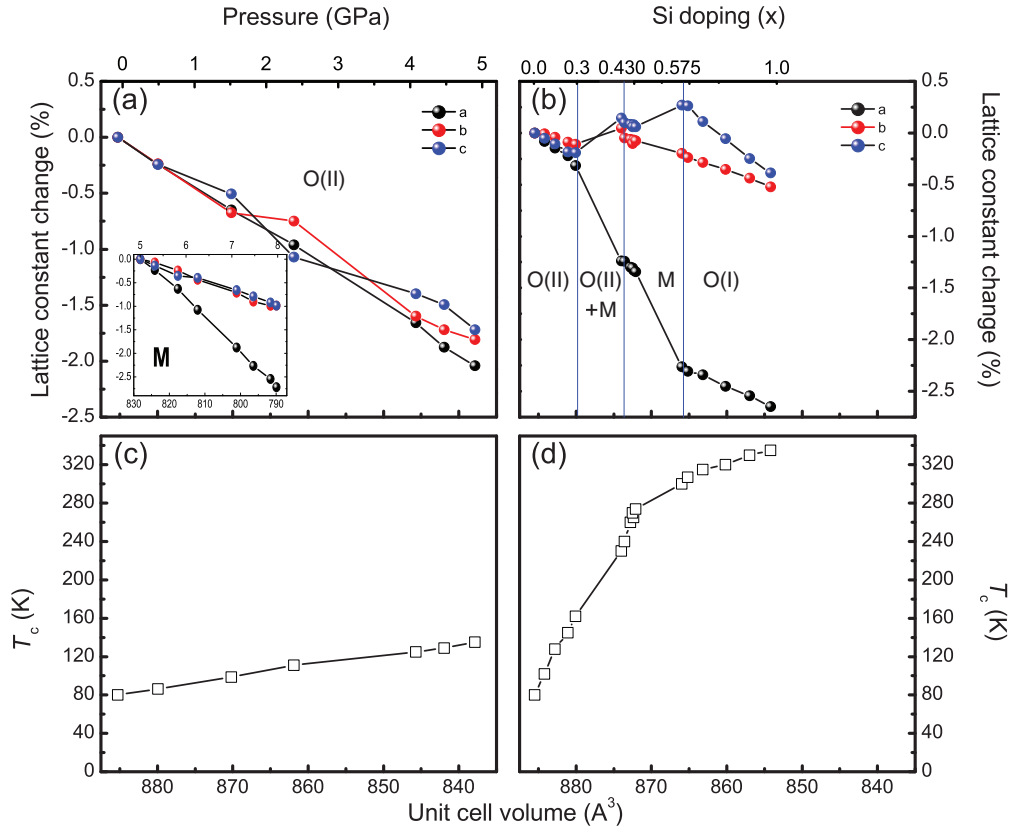


FIG. 3. (Color online) Lattice constant change and related volume change with (a) pressure at room temperature and (b) Si doping at ambient pressure for the $x = 0.125$ sample. (c) and (d) describe the T_c dependency with volume changes for pressure and Si doping, respectively, also for the $x = 0.125$ sample. All the figures [except the inset in (a)] share the same scale in volume change for the purpose of illustrating their interdependencies. The inset in (a) depicts the pressure-induced volume change in the M phase, which shares the same units [unit-cell volume (bottom), lattice constant change (left), and pressure (top)] as the main panel. Pressure data were converted from Fig. 2, and Si-doping data were taken from Ref. 15, and the diagram is marked for different phases with blue lines. The smallest volume shown in the pressure panel (a) ($\sim 837 \text{\AA}^3$) is given by $P = 5$ GPa, and the material's structure remains as $O(II)$ within this pressure range. For Si doping, the smallest volume is $\sim 852 \text{\AA}^3$ when x reaches 1 panel (b).

the open squares in panels (c) and (d) of Fig. 3. The intimate connection between structure and magnetism is a result of the strong magnetostructural coupling in these materials at the root of the giant magnetocaloric effect, namely, magnetism drives structure and structure drives magnetism. The results indicate that, although pressure and Si doping are seemingly analogous to each other, the latter is much more effective in enhancing T_c for a given volume contraction (by a factor of ~ 11). It is plausible to suggest that the Si substitution is quite efficient in inducing the structural changes in $\text{Gd}_5(\text{Si}_x\text{Ge}_{1-x})_4$ and promotes the quick rise in magnetic ordering temperature when magnetic and crystallographic lattices are coupled. A “weaker” response with pressure (compared to Si doping) is observed in both the structural only $O(II)$ - M transition at room temperature and the magnetostructural transition (at T_c), showing that electronic effects associated with Si substitution dominate over the effect of a uniform lattice contraction, even in the absence of magnetic ordering if the structural transition is possible. Yet the difference in dT_c/dV between Si substitution and pressure becomes smaller for $\text{Gd}_5(\text{Si}_x\text{Ge}_{1-x})_4$ samples with $x > 0.5$ where the $O(I)$ phase is stable and no structural transitions are observed to, at least, 350 K.

We now turn to understand the possible cause of the “sluggish” response of T_c and structural transitions to hydrostatic pressure compared to Si doping. Whereas, pressure increases the overlap between Gd $5d$ and Si $3p$ (Ge $4p$) states causing enhancement of the exchange (magnetic) interactions, Si doping modifies the p - d hybridization as a result of chemical substitution. For example, if Si $3p$ -Gd $5d$ hybridization is stronger than Ge $4p$ -Gd $5d$ hybridization, replacement of Ge atoms by Si can have a more profound effect on magnetic interactions than an attempt to “remedy” weak Ge $4p$ -Gd $5d$ orbital overlap by pressure-induced band broadening. In fact, the FM exchange strength of $\text{Gd}_5(\text{Si}_x\text{Ge}_{1-x})_4$ is critically related to the extent of Gd $5d$ and Si $3p$ (Ge $4p$) hybridizations,²⁷ so atomic substitutions either within or between the slabs have a profound effect upon the FM exchange interactions.

Experimental and theoretical XANES and XMCD spectra for Si and Ge K edges are presented in the insets of Fig. 4. Both Si and Ge display clear XMCD signals as expected from a spin-polarized conduction band with Si (Ge)- $3p$ ($4p$) and Gd $5d$ orbital characters.²⁷ The Si K -edge XANES data display a much more visible shoulder on the rising absorption

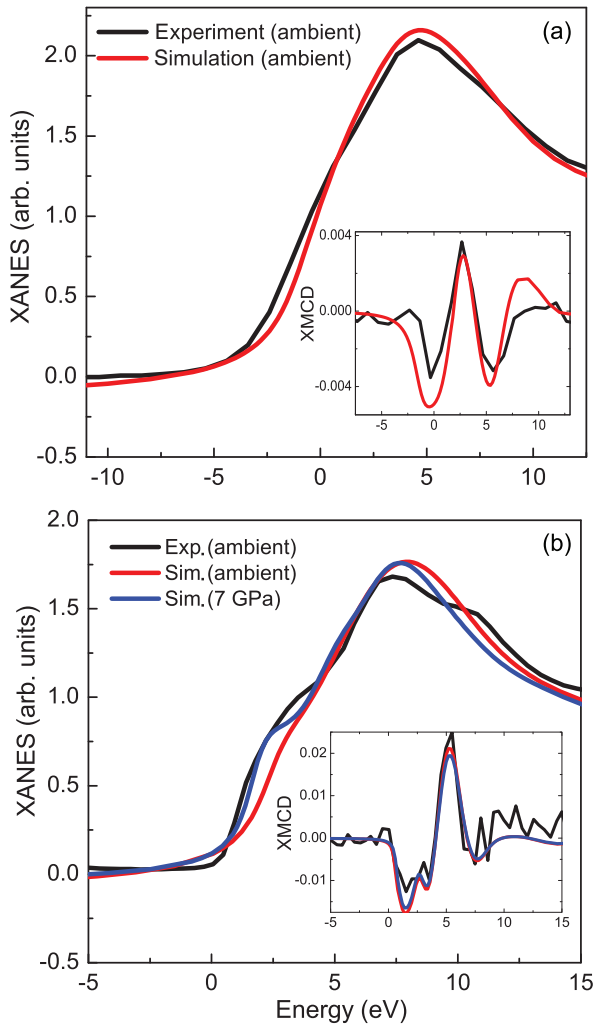


FIG. 4. (Color online) (a) Ge and (b) Si K -edge experimental and simulated XANES (main) and XMCD (inset) results of the $x = 0.5$ sample. Experimental data were collected at $T = 10$ K. The simulations were conducted using the FDMNES code^{16,17} with lattice parameters obtained by XRD at ambient and $P = 7$ GPa (only Si) pressures.

edge than seen in the Ge K -edge data. In addition, the edge-jump normalized XMCD signal at the Si K edge is approximately five times larger than at the Ge K edge. A larger Si than the Ge K -edge XMCD signal was theoretically predicted in Ref. 28 for an $x = 0.5$ monoclinic sample within the LSDA + U approximation. The shoulder in the ambient-pressure Si XANES data is not reproduced in the FDMNES simulation, which uses values of lattice parameters at ambient pressure. Interestingly, an FDMNES simulation using lattice parameters obtained by XRD at $P = 7$ GPa shows good agreement with the data, likely a result of a sizable lattice contraction at Si sites (local chemical pressure). This hypothesis is validated by Si/Ge XAFS data presented in Fig. 5 where a sizable local lattice contraction is, indeed, obtained at Si sites with significant bond-length reduction relative to Ge sites (Table I). The fitting model is able to reproduce the data with bond parameter values given in Table I. The Si-Si and Si-Gd bonds are contracted by 1.5% and 1%, respectively, relative to the macroscopic values determined

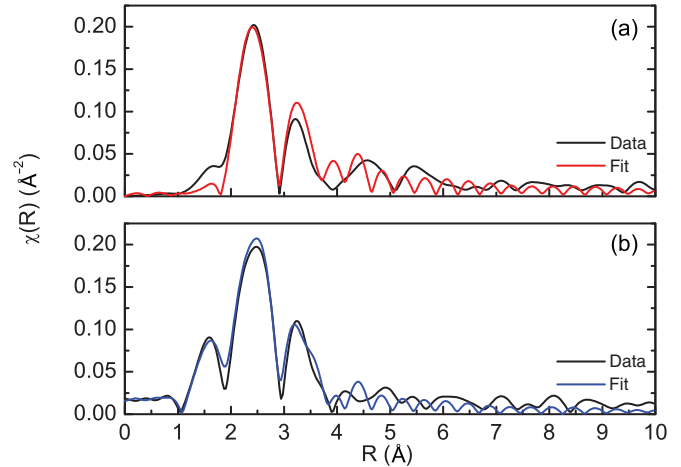


FIG. 5. (Color online) Magnitude of Fourier transform of Ge (top) and Si (bottom) K -edge XAFS spectra using the $k = [2,10]\text{-}\text{\AA}^{-1}$ and $R [2,4.2]\text{-}\text{\AA}$ ranges for the $x = 0.5$ sample at $T = 10$ K. The spectra were fitted using the crystal structure determined by XRD at 10 K.

by diffraction. This corresponds to a local volume change of approximately 3% according to $\Delta V/V = 3 \Delta R/R$ (V and R refer to molar volume and interatomic distance, respectively). Such a local lattice contraction, therefore, translates into a sizable local pressure (chemical pressure of a few gigapascals) exerted by the smaller-size Si atoms upon its immediate atomic surroundings. The FDMNES simulations are able to reproduce the on-the-edge shoulder when the local lattice structure is contracted. Based on DFT calculations of the partial density of states (DOS) discussed below, this feature is likely a result of mixing of Gd $5d$ character into the final state probed by the Si K -edge absorption process. The relevance of this local lattice contraction to the mechanism of enhanced exchange interactions with Si substitution is discussed later in the context of DFT simulations. Similarly, the larger XMCD signal at the Si K edge relative to that at the Ge K edge is related to the stronger p - d hybridization at Si sites resulting in larger induced magnetic polarization as confirmed by DFT calculations discussed below.

To further understand the relevance of p - d hybridization in enhancing the FM interactions with Si doping, we carried out band-structure calculations on the $x = 0.125$ sample. The phase diagram indicates this sample is ferromagnetic and has the orthorhombic $O(I)$ structure (all Gd-containing slabs are connected by Si/Ge-Si/Ge covalent bonds). Calculations were carried out with and without local lattice relaxation for $\text{Gd}_5\text{Si}_{0.5}\text{Ge}_{3.5}$ ($x = 0.125$) to test the effect of local lattice contraction around Si atoms. For exact Si concentration, the orthorhombic ($Pnma$) structure was converted into the equivalent triclinic ($P1$) structure so that each of the 36 atoms in the unit cell of Gd_5T_4 is formally no longer equivalent to any other atom in the same unit cell. We note here that this conversion does not affect the lattice volume and atomic positions but makes all atoms in the unit cell inequivalent and distinguishable.²⁹ Therefore, for $\text{Gd}_5\text{Si}_{0.5}\text{Ge}_{3.5}$ ($x = 0.125$), two T_2 positions out of four were assigned to Si atoms, and all other T (T_1 , T_2 , and T_3) positions were assigned to Ge atoms. Furthermore, for the calculations without lattice relaxation, the experimental lattice parameters and atomic

TABLE I. The change in the Si and Ge interatomic distances relative to those in the average structure determined by crystallography for the $x = 0.5$ sample. The results only include contributions from the first two atomic shells around the selected Si and Ge atoms.

Atom	Change in the interatomic distances		
Si	Si-Si $-0.0395 \pm 0.0074 \text{ \AA}$	Si-Ge $0.0012 \pm 0.0013 \text{ \AA}$	Si-Gd $-0.031 \pm 0.0182 \text{ \AA}$
Ge	Ge-Ge $+0.083 \pm 0.0021 \text{ \AA}$	Ge-Si $0.0012 \pm 0.0013 \text{ \AA}$	Ge-Gd $+0.004 \pm 0.003 \text{ \AA}$

positions of the $O(I)$ structure of Gd_5Ge_4 ($x = 0$) (which is ferromagnetic and is stable in applied field or pressure) were used, whereas, for the calculations with lattice relaxation, experimental lattice constants and atomic positions of the $O(I)$ phase of $Gd_5Si_{0.5}Ge_{3.5}$ ($x = 0.125$) were used as a starting point. Results for projected DOS obtained by these calculations are shown in Figs. 6(a) and 6(b), respectively. The reported Gd $5d$ DOS are averaged over all Gd atoms. It is immediately noted that the DOS of Si $3p$ and Gd $5d$ states display nearly the same energy dependence, which indicates strong $3p$ - $5d$ hybridization. This is not the case for $4p$ - $5d$ states showing poor correspondence of $4p$ and $5d$ energy-dependent DOS. We obtain magnetic moments of 0.08 and $0.04 \mu_B$ for Si and Ge, respectively (see Table II). The higher $3p$ moment of Si atoms explains the larger XMCD signal at the Si K edge relative to that at the Ge K edge (i.e., this difference in XMCD signals is not simply a result of the different matrix elements and/or core-hole lifetimes at these two edges). Figure 6(b) shows the effect of a local lattice relaxation upon the partial DOS. A bond-length reduction of $\sim 9\%$ for Si is obtained when the structure is relaxed, and

we observe a small ($\sim 9\%$) increase in spin splitting in the Gd $5d$ DOS near the Fermi level, resulting in a rather small ($\sim 4\%$) increase in the strength of exchange interaction J_{ex} . This 9% reduction in bond length is not present at the Ge sites. Although the local lattice contraction around Si sites may play a role, the driving force behind the increase in T_C (J_{ex}) with Si doping is the more effective Si $3p$ -Gd $5d$ overlap, or band alignment, compared to Ge $4p$ -Gd $5p$. Since Gd $4f$ moments couple indirectly in this metallic system through the Ruderman-Kittel-Kasuya-Yosida exchange interaction, the more effective hopping integrals achieved by Si substitution appear to be the source of enhanced ferromagnetic ordering temperature. The poor Ge $4p$ -Gd $5d$ orbital overlap can be partially compensated by inducing band broadening with applied pressure, resulting in mild increases in T_C , albeit with a much reduced efficiency than with Si doping, which yields optimal p - d band alignment.

It is noteworthy that these results were obtained by placing Si atoms at the T_2 site (intraslab), so the local lattice relaxation (chemical pressure) may be overestimated since, in the real structure, Si also populates the other two inequivalent Si/Ge crystal sites.¹⁰ However, even under this favorable chemical pressure condition, only a rather small change was observed in the Si $3p$ and Gd $5d$ DOS resulting in the small change in exchange interactions. Again this indicates that the enhanced exchange interactions are rooted in the more effective p - d hybridization achieved upon Si substitution with the chemical pressure (local lattice contraction) being a secondary effect. Clearly enhanced Si $3p$ -Gd $5d$ hybridization enables more efficient FM exchange pathways leading to a faster increase in FM order in $Gd_5(Si_xGe_{1-x})_4$ compared to that achieved by pressure-induced band broadening of the less than optimal $4p$ - $5d$ overlap.

Because of the strong magnetostructural coupling in these materials, the effectiveness of Si $3p$ -Gd $5d$ hybridization in enhancing T_C is also tied to the changes in crystal structure. Whereas, a dramatic increase in T_C is obtained for $x \leq 0.5$ (13.55 K \AA^{-3}) as the number of effective exchange pathways increases, a slowdown takes place for $x > 0.5$ (3.41 K \AA^{-3}) where a fully interconnected $O(I)$ structure with reduced compressibility is obtained at room temperature. Hence, there is a distinction between the low- x and the high- x regimes. At low x ($x < 0.5$) where the more open $O(II)$ and M structures are present at room temperature featuring a disconnected or partially connected Gd-containing slab, Si doping results in enhanced p - d hybridization and large increases in ordering temperature. The accompanying reduction in volume plays a much less important role in this x regime as seen from

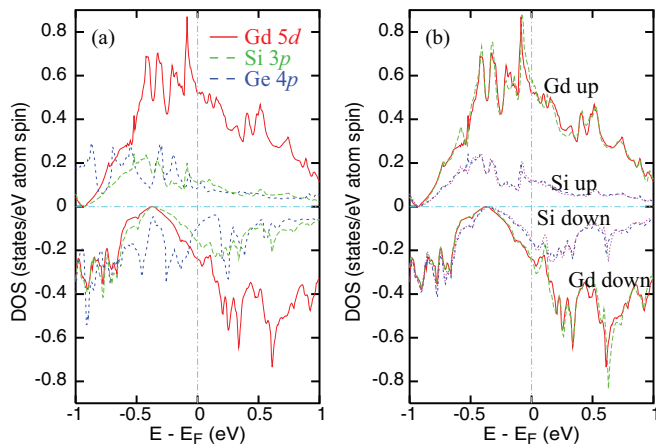


FIG. 6. (Color online) (a) Gd $5d$, Si $3p$, and Ge $4p$ density of states around the Fermi level (-1 to 1 eV) for Si and Ge atoms occupying T_2 sites (one of the intraslab sites) within the $O(I)$ - Gd_5Ge_4 structure. The Si $3p$ -Gd $5d$ hybridization is stronger in both spin directions compared to the Ge $4p$ -Gd $5d$ hybridization. (b) DOS comparison for Gd $5d$ and Si $3p$ with (green for Gd and pink for Si) and without (red for Gd and blue for Si) the local lattice relaxation (chemical pressure) effect around Si. The small changes in the spin-up density of states of Gd $5d$ at the Fermi level signifies the secondary importance of local lattice contraction compared to Gd $5d$ -Si $3p$ hybridization.

TABLE II. Magnetic moments of Gd, Ge, and Si atoms in the $O(I)$ Gd_5Ge_4 with T_2 sites occupied by Si atoms.

Sites	Gd ₁ (4c)	Gd ₂ (8d)	Gd ₃ (8d)	Ge ₃ (8d)	Ge ₁ (4c)	Si ₂ (4c)
Magnetic moments (μ_B)	7.55	7.43	7.35	0.04	0.04	0.08

pressure experiments. However, at higher x values where the three-dimensional percolation of effective exchange pathways is already achieved and the less compressible $O(I)$ structure is stabilized at all temperatures, the gains in T_C from further Si substitution are less dramatic with the relative importance of a volume contraction increasing.

IV. CONCLUSION

This paper helps unravel the mechanism behind large T_C enhancement in $Gd_5(Si_xGe_{1-x})_4$ with Si substitution. Whereas, substitution of larger Ge atoms by smaller Si atoms in the slab structure results in a lattice contraction, the main driving force behind the increase in FM exchange interactions is not this lattice contraction but rather the enhancement in $p-d$ hybridization. DFT calculations show that Si $3p$ -Gd $5d$ hybridization is stronger than Ge $4p$ -Gd $5d$ hybridization. The Si K -edge XMCD signal, being five times larger than the Ge K -edge XMCD signal, supports this result. Since $p-d$ hybridization is a critical ingredient of the indirect exchange interaction between Gd $4f$ moments in this layered structure with Gd-Si/Ge-Gd exchange pathways, the enhancement in $p-d$ hybridization with Si doping is mostly responsible for the T_C enhancements, and the accompanying volume reduction plays a secondary role. A local lattice contraction around Si atoms, larger than the macroscopic lattice contraction at low x , is clearly present based on XAFS results and FDMNES simulations of Si K -edge XANES data. However, DFT calculations show that this local lattice contraction only marginally enhances

$p-d$ hybridization and exchange interactions relative to the unrelaxed structure. Finally, an $O(II)$ to M structural phase transition is observed with applied pressures higher than 5 GPa in the paramagnetic states of $Gd_5(Si_{0.125}Ge_{0.875})_4$ at room temperature. Although the same transition is induced at room temperature with Si doping, a comparison of the corresponding unit-cell volume changes required to trigger the transition indicates that chemical substitution is a more efficient driver for the structural change than pressure—even in the absence of magnetic order—another manifestation of the dominant role of electronic effects over the lattice (volume contraction) effects. This new understanding may enable modifications in the electronic structure via doping of p and rare-earth elements at Si/Ge and Gd sites, respectively, with the potential to improve magnetocaloric properties of this and related materials.

ACKNOWLEDGMENTS

Work at National Chiao Tung University was supported by the National Science Council of Taiwan under Grant No. NSC 98-2112-M-009 022-MY3. Work at Argonne National Laboratory was supported by the U.S. Department of Energy, Office of Science, Office of Basic Energy Sciences, under Contract No. DE-AC-02-06CH11357. Work at Ames Laboratory was supported by the U.S. Department of Energy, Office of Basic Energy Science, Division of Materials Sciences and Engineering under Contract No. DE-AC02-07CH11358 with Iowa State University.

*Corresponding author: yctseng21@mail.nctu.edu.tw

¹A. Smith, C. R. H. Bahl, R. Bjork, K. Engelbrecht, K. K. Nielsen, and N. Pryds, *Adv. Eng. Mater.* **2**, 1288 (2012).

²K. A. Gschneidner, Jr., V. K. Pecharsky, and A. O. Tsokol, *Rep. Prog. Phys.* **68**, 1479 (2005).

³O. Gutfleisch, M. A. Willard, E. Bruck, C. H. Chen, S. G. Shankar, and J. P. Liu, *Adv. Mater.* **23**, 821 (2011).

⁴L. Morellon, C. Magen, P. A. Algarabel, M. R. Ibarra, and C. Ritter, *Appl. Phys. Lett.* **79**, 1318 (2001).

⁵Y. Mudryk, V. K. Pecharsky, and K. A. Gschneidner, Jr., *Z. Anorg. Allg. Chem.* **637**, 1948 (2011).

⁶Y. C. Tseng, D. Haskel, J. C. Lang, S. Sinogeikin, Ya. Mudryk, V. K. Pecharsky, and K. A. Gschneidner, Jr., *Phys. Rev. B* **76**, 014411 (2007).

⁷Y. C. Tseng, D. Haskel, J. C. Lang, Y. Mudryk, V. K. Pecharsky, and K. A. Gschneidner, Jr., *J. Appl. Phys.* **103**, 07B301 (2008).

⁸C. Magen, Z. Arnold, L. Morellon, Y. Skorokhod, P. A. Algarabel, M. R. Ibarra, and J. Kamarad, *Phys. Rev. Lett.* **91**, 207202 (2003).

⁹L. Morellon, Z. Arnold, P. A. Algarabel, C. Magen, M. R. Ibarra, and Y. Skorokhod, *J. Phys.: Condens. Matter* **16**, 1623 (2004).

¹⁰W. Choe, V. K. Pecharsky, A. O. Pecharsky, K. A. Gschneidner, Jr., V. G. Young, Jr., and G. J. Miller, *Phys. Rev. Lett.* **84**, 4617 (2000).

¹¹V. Svitlyk, G. J. Miller, and Y. Mozharivskyj, *J. Am. Chem. Soc.* **131**, 2367 (2009).

¹²L.-M. Wu, S.-H. Kim, and D.-K. Seo, *J. Am. Chem. Soc.* **127**, 15682 (2005).

¹³J. Yao, Y. Zhang, P. L. Wang, L. Lutz, G. J. Miller, and Y. Mozharivskyj, *Phys. Rev. Lett.* **110**, 077204 (2013).

¹⁴Y. Mudryk, D. Paudyal, V. K. Pecharsky, K. A. Gschneidner, Jr., S. Misra, and G. J. Miller, *Phys. Rev. Lett.* **105**, 066401 (2010).

¹⁵A. O. Pecharsky, K. A. Gschneidner, Jr., V. K. Pecharsky, and C. E. Schindler, *J. Alloys Compd.* **338**, 126 (2002).

¹⁶Y. Joly, *Phys. Rev. B* **63**, 125120 (2001).

¹⁷O. Bunău and Y. Joly, *J. Phys.: Condens. Matter* **21**, 345501 (2009).

¹⁸Y. C. Tseng, D. Haskel, N. M. Souza-Neto, Ya. Mudryk, V. K. Pecharsky, and K. A. Gschneidner, Jr., *Phys. Rev. B* **78**, 214433 (2008).

¹⁹D. Haskel, Y. C. Tseng, J. C. Lang, and S. Sinogeikin, *Rev. Sci. Instrum.* **78**, 083904 (2007).

- ²⁰S. I. Zabinsky, J. J. Rehr, A. Ankudinov, R. C. Albers, and M. J. Eller, *Phys. Rev. B* **52**, 2995 (1995).
- ²¹<http://cars9.uchicago.edu/ifeffit/>.
- ²²Y. Ding, D. Haskel, S. G. Ovchinnikov, Y.-C. Tseng, Y. S. Orlov, J. C. Lang, and H.-k. Mao, *Phys. Rev. Lett.* **100**, 045508 (2008).
- ²³A. P. Hammersley, S. O. Svensson, M. Hanfland, A. N. Fitch, and D. Hausermann, *High Press. Res.* **14**, 235 (1996).
- ²⁴L. B. McCusker, R. B. Von Dreele, D. E. Cox, D. Louër, and P. Scardi, *J. Appl. Crystallogr.* **32**, 36 (1999).
- ²⁵D. Paudyal, V. K. Pecharsky, K. A. Gschneidner, Jr., and B. N. Harmon, *Phys. Rev. B* **73**, 144406 (2006).
- ²⁶D. Paudyal, Y. Mudryk, V. K. Pecharsky, and K. A. Gschneidner, Jr., *Phys. Rev. B* **84**, 014421 (2011).
- ²⁷D. Haskel, Y. B. Lee, B. N. Harmon, Z. Islam, J. C. Lang, G. Srajer, Y. Mudryk, K. A. Gschneidner, Jr., and V. K. Pecharsky, *Phys. Rev. Lett.* **98**, 247205 (2007).
- ²⁸B. N. Harmon and V. N. Antonov, *J. Appl. Phys.* **93**, 4678 (2003).
- ²⁹D. Paudyal, V. K. Pecharsky, and K. A. Gschneidner, Jr., *J. Phys.: Condens. Matter.* **20**, 235235 (2008).